Information Content of the Parity-Violating Asymmetry in ^{208}Pb

Paul-Gerhard Reinhard,[1] Xavier Roca-Maza,[2] and Witold Nazarewicz[3]
[1]Institut für Theoretische Physik, Universität Erlangen, Erlangen, Germany
[2]Dipartimento di Fisica "Aldo Pontremoli," Università degli Studi di Milano, 20133 Milano, Italy and INFN, Sezione di Milano, 20133 Milano, Italy
[3]Facility for Rare Isotope Beams and Department of Physics and Astronomy, Michigan State University, East Lansing, Michigan 48824, USA

(Received 31 May 2021; accepted 27 October 2021; published 29 November 2021)

The parity-violating asymmetry A_{PV} in ^{208}Pb, recently measured by the PREX-2 Collaboration, is studied using modern relativistic (covariant) and nonrelativistic energy density functionals. We first assess the theoretical uncertainty on A_{PV} which is intrinsic to the adopted approach. To this end, we use quantified functionals that are able to accommodate our previous knowledge on nuclear observables such as binding energies, charge radii, and the dipole polarizability α_D of ^{208}Pb. We then add the quantified value of A_{PV} together with α_D to our calibration dataset to optimize new functionals. Based on these results, we predict a neutron skin thickness in ^{208}Pb $r_{\mathrm{skin}} = 0.19 \pm 0.02$ fm and the symmetry-energy slope $L = 54 \pm 8$ MeV. These values are consistent with other estimates based on astrophysical data and are significantly lower than those recently reported using a particular set of relativistic energy density functionals. We also make a prediction for the A_{PV} value in ^{48}Ca that will be soon available from the CREX measurement.

DOI: 10.1103/PhysRevLett.127.232501

Introduction.—The recent measurement of the parity-violating asymmetry A_{PV} at transferred momentum $q = 0.3978/\mathrm{fm}$ in ^{208}Pb by the PREX-2 Collaboration [1] provided a highly anticipated observable that can inform models of nuclei and nuclear matter. In a separate theoretical paper [2], implications of the PREX-2 result on nuclear properties and the equation of state of neutron-rich matter have been discussed within a specific class of relativistic energy density functionals (EDFs). The authors relate the measured A_{PV} to r_{skin} and deduce from that a rather large symmetry-energy slope parameter $L = 106 \pm 37$ MeV and a large neutron skin thickness in ^{208}Pb $0.21 \lesssim r_{\mathrm{skin}} \lesssim 0.31$ fm. The mean values of these quantities systematically overestimate the currently accepted limits ($J = [28.5, 34.9]$ MeV, $L = [30.6, 86.8]$ MeV [3–5], and $r_{\mathrm{skin}} = [0.13, 0.19]$ fm [6–8]).

We emphasize the fact that the new experimental information provided by PREX-2 Collaboration is the A_{PV} measured at a specific kinematic condition. Other nuclear quantities of interest reported in [1,2], such as the neutral weak form factor, neutron skin thickness, interior weak density, interior baryon density, and symmetry-energy parameters, become accessible only via theoretical models.

The question addressed in this Letter is whether the PREX-2 value of A_{PV} creates a principle tension with other data and models, as claimed in [2]. The strategy is, first, to study A_{PV} directly rather than nonobservable quantities, and second, to employ a broad set of structurally different EDFs together with a statistical analysis [9] to estimate the uncertainty on A_{PV} intrinsic to each EDF as well as the correlation with other observables. In particular, we consider the relation with the electric dipole polarizability α_D in ^{208}Pb which is known to be strongly correlated with r_{skin} and weak form factor [10–12] and for which independent experimental data exist [8,13]. All EDFs under consideration show a clear correlation between A_{PV} and α_D and indicate a possible incompatibility of their current values. We extend the analysis to other observables as neutron skins, bulk symmetry energy, and its slope, and we make predictions for A_{PV} in ^{48}Ca at the CREX kinematics [14].

The parity-violating asymmetry.—A_{PV} can be obtained experimentally from longitudinally polarized elastic electron scattering [15] as

$$A_{\mathrm{PV}}(Q^2) = \frac{d\sigma_R/d\Omega - d\sigma_L/d\Omega}{d\sigma_R/d\Omega + d\sigma_L/d\Omega}, \tag{1}$$

where $d\sigma_L/d\Omega$ ($d\sigma_R/d\Omega$) is the differential cross section for the scattering of left (right) handed electrons, Ω is the solid angle, and Q^2 is the squared transferred four momentum. The scattering cross sections in (1), for a heavy nucleus, must be computed taking into account Coulomb distortions [16,17]. To this end, we have modified the Dirac partial-wave code ELSEPA [18] to deal with parity nonconserving potentials. Actually, the distribution of scattering angles in the PREX-2 experiment has a non-negligible width which we take into account by considering the PREX-2 acceptance function, see Supplemental Material (SM) [19] for details.

To gain insight into structure of the parity-violating asymmetry, it is useful to inspect the plane wave Born approximation expression for $A_{\rm PV}$: [15]

$$A_{\rm PV}(Q^2) \approx -\frac{G_F Q^2 Q^{(W)}_{N,Z}}{4\sqrt{2}\pi\alpha Z}\frac{F_W(q)}{F_C(q)}, \tag{2}$$

where $q = \sqrt{Q^2}$, $G_F = 1.1663787 \times 10^{-5}/\mathrm{GeV}^2$ is the Fermi coupling constant, F_W the weak form factor, F_C is the charge form factor, and $Q^{(W)}_{N,Z}$ is the weak charge of the nucleus with N neutrons and Z protons. Both F_W and F_C are normalized to one. Since F_C primarily depends on protons and F_W on neutrons, $A_{\rm PV}$ decreases linearly with $r_{\rm skin}$ at low Q^2, also when Coulomb distortions are taken into account [17]. Consequently this observable can be used to infer information on $r_{\rm skin}$.

Even if exploited at a single kinematic condition, $A_{\rm PV}$ is one of the most promising observables to probe neutrons in nuclei since it is based on the well known electroweak interaction. Other promising observables (cf. Refs. [32–34]) sensitive to the neutron distribution in nuclei include the dipole polarizability α_D [8,13], which we shall discuss in this Letter.

Error budget for $A_{\rm PV}$.—In Table I, we list the nucleonic parameters that are used for the calculation of the nucleon electromagnetic and weak form factors and $A_{\rm PV}$, see SM [19] for details.

Most parameters in Table I are given with errors either from experimental analysis or compilation of different sources. To estimate how these errors propagate to the prediction of $A_{\rm PV}$ on a test calculation, we assume a Gaussian profile for the distribution of each parameter to sample the variance in $A_{\rm PV}$. The result is shown in Fig. 1. The first six entries show the impact of each parameter separately. Considerable contributions come only from the strength of the s quark and, dominantly, from $Q^{(W)}_{N,Z}$. The entry "sum 1–6" shows the total uncertainty from the first six entries accumulated by the Gaussian law of error propagation.

There are also uncertainties on the predictions of the theoretical models (see below) stemming from the empirical calibration of the model parameters. The last two entries in Fig. 1 show them (thin blue bars) for two typical model parametrizations discussed below together with the errors from the nucleonic parameters (thick red bars). Both theoretical predictions are compatible, within errors, with the upper edge of the experimental uncertainty of the PREX-2 measurement [1].

Theoretical models.—There exists a variety of nuclear EDFs in the literature (for a review, see, e.g., [43,44]). They differ in their structure and in the way there were calibrated. We use here several families of EDFs having different functional form and provide in similar fashion a set of parametrizations with systematically varied symmetry energy J, while maintaining isoscalar properties and an overall good quality in their predictions. This is of particular interest when studying an observable like $A_{\rm PV}$ which, being related to the differences between the weak and electric charge densities, is predominantly sensitive to the isovector channel of the EDFs [10]. The families of EDFs considered in the survey are: FSU—based on the traditional nonlinear Walecka model [45] specially devised to minimally improve its flexibility on the isovector channel [46]; DD and PC—extended RMF models with more flexibility due to density-dependent coupling

TABLE I. Final choice of the parameters entering the calculation of the weak form factor and $A_{\rm PV}$: the electric proton $\langle r_p^2\rangle$ and neutron $\langle r_n^2\rangle$ radii; the magnetic dipole moments, μ_p and μ_n; the strange quark electric coupling ρ_s and the strange quark magnetic moment κ_s; the weak charge of neutrons $Q_n^{(W)}$ and protons $Q_p^{(W)}$; and the total weak charge of ^{208}Pb $Q^{(W)}_{126,82}$.

Parameter	Value	Ref.
$\langle r_p^2\rangle$ (fm^2)	0.726 ± 0.019	[35]
$\langle r_n^2\rangle$ (fm^2)	-0.1161 ± 0.0022	[36]
μ_p	2.792 847	[36]
μ_n	-1.9130	[36]
$Q_p^{(W)}$	0.0713 ± 0.0001	[37,38]
$Q_n^{(W)}$	-0.9888 ± 0.0011	[37,38]
ρ_s	-0.24 ± 0.70	[39,40]
κ_s	-0.017 ± 0.004	[41]
$Q^{(W)}_{126,82}$	-117.9 ± 0.3	[1,42]

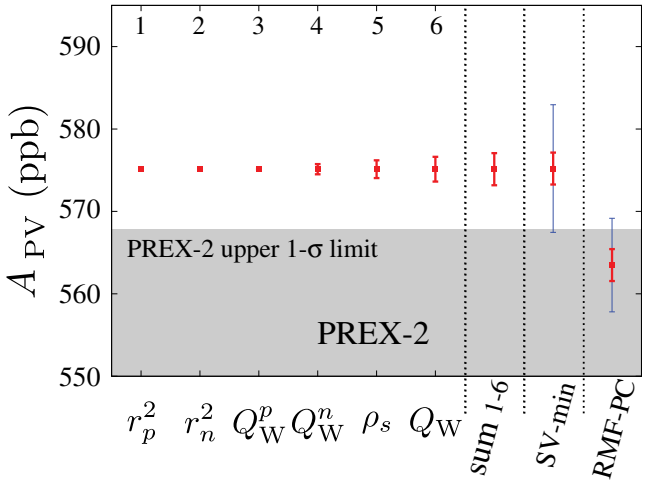

FIG. 1. Uncertainty budget for $A_{\rm PV}$. First six entries labeled 1–6: the effect of the errors on the parameters in Table I on the uncertainty on $A_{\rm PV}$. The resulting total uncertainty due to coupling constants is labeled "sum 1–6." The quantified predictions of $A_{\rm PV}$ with SV-min and RMF-PC models (thin bars), which include statistical model uncertainties related to neutron and proton point densities and the coupling-constant uncertainty. The experimental value of $A_{\rm PV}$ is 550 ± 17.9 ppb [1]. The gray band marks the corresponding upper 1-sigma confidence interval.

constants. DD employs the traditional finite-range meson-exchange fields [47] while PC uses point couplings [48]; the series of SV [49] and SAMi [50] parametrizations belong to the widely used nonrelativistic Skyrme EDFs; the RD series is a variant of the Skyrme EDFs with a different form of density dependence [51]. Four of the families (SV, RD, PC, and DD) are calibrated to exactly the same large set of ground observables: binding energies, charge radii, diffraction radii, and surface thicknesses in semimagic, spherical nuclei [49], plus a systematically scanned constraint on symmetry energy J. The differences between the results of these EDF families show the impact of the EDF form. The calibration is done by means of the standard linear regression, which also provides information on uncertainties and statistical correlations between observables [9,12]. The other two families (FSU and SAMi) are calibrated to different datasets with different bias. The SAMi functionals, e.g., have been optimized with the focus on spin-isospin resonances. We include these functionals to probe the impact of calibration strategy. However, we checked that the performance for the reference nucleus, ^{208}Pb, is roughly comparable for all parametrizations used, see the SM for details [19]. The intermodel comparison helps quantifying the systematic theoretical error.

Tension between the PREX-2 result and electric dipole polarizability.—The dipole polarizability α_D in nuclei, directly related to the photoabsorption cross section, provides an excellent constraint on $r_{\rm skin}$ [7,32,52]. The measurements of α_D have been carried out for a number of nuclei, in particular for ^{208}Pb [13] and ^{48}Ca [53]. These experiments provide a reliable information on the photoabsorption cross section up to about 20 MeV. Small high-energy contributions to α_D require careful modeling of the quasideuteron effect [54,55], which motivated the correction from the original value 20.1 ± 0.6 fm^3 [13] to the value 19.6 ± 0.6 fm^3 used here (cf. Ref. [8]).

Figure 2 shows the predicted values of $A_{\rm PV}$ versus α_D obtained with the set of covariant and nonrelativistic EDFs. The figure illustrates a nearly linear trend of $A_{\rm PV}$ versus α_D with the same slope for all models, but slightly different offset mostly depending on different values of the symmetry-energy coefficient J predicted by the EDFs [7]. The parametrizations SV-min and RMF-PC stem from unconstrained fits to ground state data and their results are shown with the predicted 1-sigma error ellipses, which align along the average trend. This indicates that the statistical uncertainties of SV-min and RMF-PC are consistent with the systematic intermodel trends. It is apparent that there is only one model which is able to reproduce simultaneously $A_{\rm PV}$ and α_D within the experimental 1-σ error bands. The figure demonstrates therefore some tension: the models that are consistent with α_D yield large values of $A_{\rm PV}$ that are outside the 1-sigma limit of PREX-2 while the models that reproduce $A_{\rm PV}$ yield the values of α_D that are well outside the experimental bounds. The single

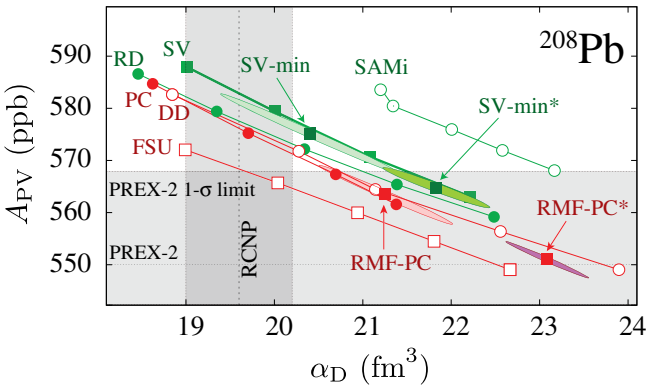

FIG. 2. $A_{\rm PV}$ versus α_D in ^{208}Pb for a set of covariant (red) and nonrelativistic (green) EDFs. Sets with systematically varied symmetry energy J are connected by lines. (Note that α_D increases as a function of J.) The SV-min, SV-min*, RMF-PC, and RMF-PC* results are shown together with their 1-sigma error ellipses. The experimental values of α_D [8,13] and $A_{\rm PV}$ [1] are indicated together with their 1-sigma error bars.

model that seems to be consistent with the current limits on $A_{\rm PV}$ and α_D is the FSU EDF with $J \sim 32$ MeV and $L \sim 60$ MeV. Its value of L is consistent with the other models in this survey but stays off the value $L = 106 \pm 37$ MeV advocated in Ref. [2]. Unfortunately, when it comes to other observables for ^{208}Pb, such as binding energy and charge radius, the performance of FSU models is inferior to the other EDFs discussed here, see [19] for details.

New EDFs constrained on $A_{\rm PV}$ and α_D.—Figure 2 shows that the unconstrained fits, SV-min for the Skyrme functionals and RMF-PC for the RMF family, form a compromise between $A_{\rm PV}$ and α_D with the Skyrme functional tending toward the mean value of α_D and the RMF—toward the mean value of $A_{\rm PV}$. To explore the compromise more systematically, we have fitted two new parametrizations taking the same set of ground state data from [49] as were used for SV-min and PC-min and adding the experimental values for $A_{\rm PV}$ and α_D to the dataset of constraining observables. The relative weight of these two new data points is regulated by taking for the adopted errors the uncertainty of the model predictions from the unconstrained fits (this amounts to 7 ppb/5.7 ppb for $A_{\rm PV}$ and 1.0 fm^3/0.7 fm^3 for α_D for SV-min/PC-min). We note that our adopted errors for $A_{\rm PV}$ are close to the systematic error of PREX-2 measurement, which is 8 ppb, and well below the statistical error of 16 ppb. The resulting parametrizations, called SV-min* and RMF-PC*, stay on the general trend and move toward the mean value of $A_{\rm PV}$. We also carried out optimizations assuming the total experimental uncertainty of PREX-2 of 17.9 ppb, dominated by statistics, for the adopted error of $A_{\rm PV}$. The models calibrated under such assumption provide practically the same results as SV-min and RMF-PC because the prior uncertainty on $A_{\rm PV}$ is so large that the information content of this variable in this calibration scenario is low. Based on

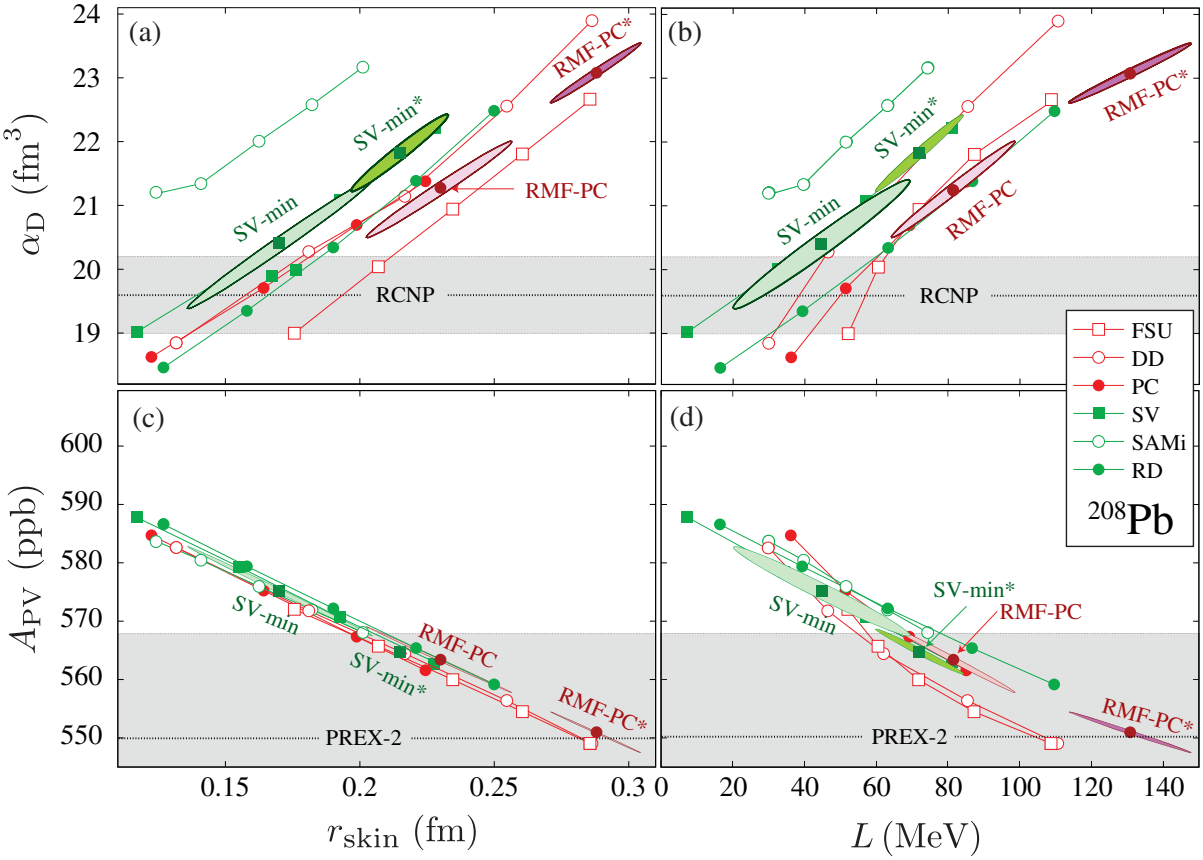

FIG. 3. A_{PV} [panels (c),(d)] and α_D in ^{208}Pb [panels (a),(b)] versus neutron skin (left panels) and slope of symmetry energy L (right panels), for the same set of EDFs as in Fig. 2. The experimental ranges of α_D [8,13] and A_{PV} [1] are marked. The values of r_{skin} (in fm) obtained in our models are 0.17 ± 0.03 for SV-min; 0.22 ± 0.02 for SV-min*; 0.23 ± 0.03 for RMF-PC; and 0.29 ± 0.02 for RMF-PC*. The values of L (in MeV) are 45 ± 25 for SV-min; 72 ± 12 for SV-min*; 82 ± 17 for RMF-PC; and 128 ± 17 for RMF-PC*.

Fig. 2 we conclude that SV-min* and RMF-PC* yield results that are consistent with the current data on A_{PV}. On the other hand, the model RMF-PC*, while closest to the mean value of A_{PV}, has $\alpha_D = 23.1$ fm^3 which is clearly inconsistent with the measured value $\alpha_D = 19.6 \pm 0.6$ fm^3.

Symmetry energy and neutron skin.—Over the years, strong correlations have been established between r_{skin} in heavy nuclei and various nuclear matter properties. Of particular importance, is the correlation of r_{skin} with the symmetry energy at the saturation point J [32,56–58] and with the slope of the bulk symmetry energy L [57,59,60], see also Refs. [11,61–63]. In addition to numerous intermodel comparisons published, strong correlation between L, J, and r_{skin} in medium-mass and heavy spherical closed-shell nuclei has been demonstrated by means of the statistical correlation analysis [32,64,65]. One can conclude from the previous body of work that the models with large symmetry-energy parameters J and L predict smaller A_{PV} and large α_D, as indicated by the trend shown in Fig. 2. Also, the relativistic models tend to yield stiffer (larger value of L) neutron equation of state compared to the nonrelativistic models [6,62].

Figure 3 shows the model predictions as functions of r_{skin} and L for the models employed. Our result for J can be found in SM [19]. There is one more important aspect in Fig. 3(c): the trend of A_{PV} versus r_{skin} has the by far smallest spread within the families of the models employed. This intimate connection is also confirmed by statistical analysis for SV and RMF-PC EDFs: the correlation coefficient between A_{PV} and r_{skin} is 99.9%.

It is interesting to compare the values of symmetry energy predicted in this work with the most current estimates based on astrophysical constraints [5,66,67] and chiral effective field theory [68,69]. To this end, we go back to Fig. 2 and search for those parametrizations in each series (SV, RD, PC, DD) which come closest to the intercept of the RNCP and PREX-2 band. Specifically, the "best compromise" parametrization is determined by drawing a line from the intercept of the mean RNCP and PREX-2 lines through the intercept of the upper limits of their error bands and checking where this line crosses the trend-trajectories of the various model families. The resulting intermodel average is our prediction and the corresponding variance becomes our estimate for the systematic

model error. For the symmetry energy, this procedure yields $J = 32 \pm 1$ MeV. This value is consistent with the estimates based on astrophysical constraints $J = 31.6 \pm 2.7$ MeV [5] (see also Refs. [3,4,66,67]) and chiral effective field theory 31.7 ± 1.1 MeV [68] and 34 ± 3 MeV [69], while the estimate $J = 38.1 \pm 4.7$ MeV of Ref. [2] differs much more.

The symmetry-energy slope is determined with larger uncertainty: $L = 54 \pm 8$ MeV. This value is comparable with $L = 57.7 \pm 19$ MeV [66], $L = 59.8 \pm 4.1$ MeV [68], and 58 ± 19 MeV [69]. The analysis of [2] using specific relativistic EDFs yields a fairly large value of $L = 106 \pm 37$ MeV.

The models compatible with the experimental α_D for ^{208}Pb predict $r_{\rm skin}$ in the range 0.13–0.19 fm [6–8], i.e., in the range of SV-min values. Our expectation for $r_{\rm skin}$ from the present analysis is 0.19 ± 0.02 fm, i.e., a mean value that is lower than the estimate 0.283 ± 0.071 fm of Ref. [1].

CREX measurement of $A_{\rm PV}$ in ^{48}Ca.—The CREX measurement will soon provide the highly anticipated data on $A_{\rm PV}$ in ^{48}Ca [14]. In SM [19] we discuss our predictions at the kinematic point of CREX $Q^2 = 0.03$ GeV^2. Considering our results for ^{208}Pb, we chose the value for $A_{\rm PV}(^{48}{\rm Ca})$ close to the prediction of SV-min with a slight bias toward SV-min*, which amounts to 2400 ± 60 ppb. We note that our predictions of $\alpha_D(^{48}{\rm Ca})$ are in a slight conflict with the current experimental estimate [53].

Summary and perspectives.—For the quantified EDFs, there exists a tension between $A_{\rm PV}$ and α_D. The functionals SV-min, SV-min*, and RMF-PC offer a reasonable compromise between the data on $A_{\rm PV}$ and α_D; they also perform well for other properties of ^{208}Pb. According to our analysis, the significant 1-sigma uncertainty of PREX-2 value of $A_{\rm PV}$ makes it difficult to use this observable as a meaningful constraint on the isovector sector of current EDFs. On the other hand, our estimated model uncertainty on $A_{\rm PV}$, 6–7 ppb is close to the estimated systematic error of PREX-2 of 8 ppb. We recommend this value for the future calibration studies. In this respect, the anticipated precision measurements of $A_{\rm PV}$ and α_D will be extremely useful for the calibration of nuclear models.

As stated in [2], their values of J, L, and $r_{\rm skin}$ in ^{208}Pb "systematically overestimate current limits based on both theoretical approaches and experimental measurements." On the other hand, the values predicted in this work are significantly lower: they are consistent with much of the previous work and the recent astrophysical estimates.

Useful discussions with R. J. Furnstahl, C. J. Horowitz, K. S. Kumar, and D. R. Phillips are gratefully acknowledged. X. R. M. thanks J. Erler and M. Gorchtein for useful discussions on the weak charge of ^{208}Pb. This material is based upon work supported by the U.S. Department of Energy, Office of Science, Office of Nuclear Physics under Awards No. DE-SC0013365 and No. DE-SC0018083 (NUCLEI SciDAC-4 Collaboration).

[1] D. Adhikari *et al.* (PREX Collaboration), Accurate Determination of the Neutron Skin Thickness of ^{208}Pb through Parity-Violation in Electron Scattering, Phys. Rev. Lett. **126**, 172502 (2021).
[2] B. T. Reed, F. J. Fattoyev, C. J. Horowitz, and J. Piekarewicz, Implications of PREX-2 on the Equation of State of Neutron-Rich Matter, Phys. Rev. Lett. **126**, 172503 (2021).
[3] J. M. Lattimer and Y. Lim, Constraining the symmetry parameters of the nuclear interaction, Astrophys. J. **771**, 51 (2013).
[4] B.-A. Li and X. Han, Constraining the neutron-proton effective mass splitting using empirical constraints on the density dependence of nuclear symmetry energy around normal density, Phys. Lett. B **727**, 276 (2013).
[5] M. Oertel, M. Hempel, T. Klähn, and S. Typel, Equations of state for supernovae and compact stars, Rev. Mod. Phys. **89**, 015007 (2017).
[6] J. Piekarewicz, B. K. Agrawal, G. Colò, W. Nazarewicz, N. Paar, P.-G. Reinhard, X. Roca-Maza, and D. Vretenar, Electric dipole polarizability and the neutron skin, Phys. Rev. C **85**, 041302(R) (2012).
[7] X. Roca-Maza, M. Brenna, G. Colò, M. Centelles, X. Viñas, B. K. Agrawal, N. Paar, D. Vretenar, and J. Piekarewicz, Electric dipole polarizability in ^{208}Pb: Insights from the droplet model, Phys. Rev. C **88**, 024316 (2013).
[8] X. Roca-Maza, X. Viñas, M. Centelles, B. K. Agrawal, G. Colò, N. Paar, J. Piekarewicz, and D. Vretenar, Neutron skin thickness from the measured electric dipole polarizability in ^{68}Ni, ^{120}Sn, and ^{208}Pb, Phys. Rev. C **92**, 064304 (2015).
[9] J. Dobaczewski, W. Nazarewicz, and P.-G. Reinhard, Error estimates of theoretical models: A guide, J. Phys. G **41**, 074001 (2014).
[10] P.-G. Reinhard, J. Piekarewicz, W. Nazarewicz, B. K. Agrawal, N. Paar, and X. Roca-Maza, Information content of the weak-charge form factor, Phys. Rev. C **88**, 034325 (2013).
[11] W. Nazarewicz, P. G. Reinhard, W. Satuła, and D. Vretenar, Symmetry energy in nuclear density functional theory, Eur. Phys. J. A **50**, 20 (2014).
[12] J. Erler and P.-G. Reinhard, Error estimates for the Skyrme-Hartree-Fock model, J. Phys. G **42**, 034026 (2015).
[13] A. Tamii, I. Poltoratska, P. von Neumann-Cosel, Y. Fujita, T. Adachi *et al.*, Complete Electric Dipole Response and the Neutron Skin in ^{208}Pb, Phys. Rev. Lett. **107**, 062502 (2011).
[14] S. Riordan *et al.*, CREX: Parity violating measurement of the weak charge distribution of ^{48}Ca to 0.02 fm accuracy, JLAB-PR- 40-12-004, TJNAF, 2013.
[15] C. J. Horowitz, S. J. Pollock, P. A. Souder, and R. Michaels, Parity violating measurements of neutron densities, Phys. Rev. C **63**, 025501 (2001).
[16] C. J. Horowitz, Parity violating elastic electron scattering and Coulomb distortions, Phys. Rev. C **57**, 3430 (1998).

[17] X. Roca-Maza, M. Centelles, X. Viñas, and M. Warda, Neutron Skin of ^{208}Pb, Nuclear Symmetry Energy, and the Parity Radius Experiment, Phys. Rev. Lett. **106**, 252501 (2011).

[18] F. Salvat, A. Jablonski, and C. J. Powell, ELSEPA-Dirac partial-wave calculation of elastic scattering of electrons and positrons by atoms, positive ions and molecules, Comput. Phys. Commun. **165**, 157 (2005).

[19] See Supplemental Material at http://link.aps.org/supplemental/10.1103/PhysRevLett.127.232501 for more details on the angular averaging of A_{PV}, the weak charge of ^{208}Pb, electromagnetic and weak form factors, EDFs used in this Letter, and predictions for the symmetry energy coefficient J in ^{208}Pb and the electric dipole polarizability in ^{48}Ca, which includes Refs. [20–31].

[20] D. Antypas, A. Fabricant, J. E. Stalnaker, K. Tsigutkin, V. V. Flambaum, and D. Budker, Isotopic variation of parity violation in atomic ytterbium, Nat. Phys. **15**, 120 (2019).

[21] J. Erler and S. Su, The weak neutral current, Prog. Part. Nucl. Phys. **71**, 119 (2013).

[22] J. Erler, M. Gorchtein, O. Koshchii, C.-Y. Seng, and H. Spiesberger, Reduced uncertainty of the axial γZ-box diagram correction to the proton's weak charge, Phys. Rev. D **100**, 053007 (2019).

[23] V. A. Dzuba, J. C. Berengut, V. V. Flambaum, and B. Roberts, Revisiting Parity Nonconservation in Cesium, Phys. Rev. Lett. **109**, 203003 (2012).

[24] P.-G. Reinhard and W. Nazarewicz, Nuclear charge densities in spherical and deformed nuclei: Toward precise calculations of charge radii, Phys. Rev. C **103**, 054310 (2021).

[25] J. Friedrich and N. Vögler, The salient features of charge density distribution of medium and heavy even-even nuclei determined from a systematic analysis of elastic electron scattering form factors, Nucl. Phys. **A373**, 192 (1982).

[26] J. L. Friar and J. W. Negele, Theoretical and experimental determination of nuclear charge distributions, Adv. Nucl. Phys. **8**, 219 (1975).

[27] J. Kelly, Nucleon charge and magnetization densities from Sachs form factors, Phys. Rev. C **70**, 068202 (2004).

[28] G. Simon, C. Schmitt, F. Borkowski, and V. Walther, Absolute electron-proton cross sections at low momentum transfer measured with a high pressure gas target system, Nucl. Phys. **A333**, 381 (1980).

[29] P. Klüpfel, J. Erler, P.-G. Reinhard, and J. A. Maruhn, Systematics of collective correlation energies from self-consistent mean-field calculations, Eur. Phys. J. A **37**, 343 (2008).

[30] C. J. Horowitz, K. S. Kumar, and R. Michaels, Electroweak measurements of neutron densities in CREX and PREX at JLab, USA, Eur. Phys. J. A **50**, 48 (2014).

[31] Z. Lin and C. J. Horowitz, Full weak-charge density distribution of ^{48}Ca from parity-violating electron scattering, Phys. Rev. C **92**, 014313 (2015).

[32] P.-G. Reinhard and W. Nazarewicz, Information content of a new observable: The case of the nuclear neutron skin, Phys. Rev. C **81**, 051303(R) (2010).

[33] X. Roca-Maza and N. Paar, Nuclear equation of state from ground and collective excited state properties of nuclei, Prog. Part. Nucl. Phys. **101**, 96 (2018).

[34] X. Roca-Maza, G. Colò, and H. Sagawa, Nuclear Symmetry Energy and the Breaking of the Isospin Symmetry: How Do They Reconcile with Each Other? Phys. Rev. Lett. **120**, 202501 (2018).

[35] H. Atac, M. Constantinou, Z. E. Meziani, M. Paolone, and N. Sparveris, Charge radii of the nucleon from its flavor dependent Dirac form factors, Eur. Phys. J. A **57**, 65 (2021).

[36] M. Tanabashi *et al.* (Particle Data Group), Review of particle physics, Phys. Rev. D **98**, 030001 (2018).

[37] C. J. Horowitz and J. Piekarewicz, Impact of spin-orbit currents on the electroweak skin of neutron-rich nuclei, Phys. Rev. C **86**, 045503 (2012).

[38] M. Hoferichter, J. Menéndez, and A. Schwenk, Coherent elastic neutrino-nucleus scattering: EFT analysis and nuclear responses, Phys. Rev. D **102**, 074018 (2020).

[39] A. Acha *et al.* (HAPPEX Collaboration), Precision Measurements of the Nucleon Strange Form Factors at $Q^2 \sim 0.1$ GeV^2, Phys. Rev. Lett. **98**, 032301 (2007).

[40] J. Liu, R. D. McKeown, and M. J. Ramsey-Musolf, Global analysis of nucleon strange form factors at low Q^2, Phys. Rev. C **76**, 025202 (2007).

[41] C. Alexandrou, S. Bacchio, M. Constantinou, J. Finkenrath, K. Hadjiyiannakou, K. Jansen, and G. Koutsou, Nucleon strange electromagnetic form factors, Phys. Rev. D **101**, 031501(R) (2020).

[42] J. Erler and M. Gorchtein (private communication).

[43] M. Bender, P.-H. Heenen, and P.-G. Reinhard, Self-consistent mean-field models for nuclear structure, Rev. Mod. Phys. **75**, 121 (2003).

[44] N. Schunck *et al.*, *Energy Density Functional Methods for Atomic Nuclei* (IOP Publishing, London, 2019), pp. 2053–2563, https://doi.org/10.1088/2053-2563/aae0ed.

[45] B. D. Serot and J. D. Walecka, The relativistic nuclear many-body problem, in *Advances in Nuclear Physics*, edited by J. W. Negele and E. Vogt (Plenum Press, New York, 1986), Vol. 16.

[46] J. Piekarewicz, Pygmy resonances and neutron skins, Phys. Rev. C **83**, 034319 (2011).

[47] T. Nikšić, D. Vretenar, P. Finelli, and P. Ring, Relativistic Hartree-Bogoliubov model with density-dependent meson-nucleon couplings, Phys. Rev. C **66**, 024306 (2002).

[48] T. Nikšić, D. Vretenar, and P. Ring, Relativistic nuclear energy density functionals: Adjusting parameters to binding energies, Phys. Rev. C **78**, 034318 (2008).

[49] P. Klüpfel, P.-G. Reinhard, T. J. Bürvenich, and J. A. Maruhn, Variations on a theme by Skyrme: A systematic study of adjustments of model parameters, Phys. Rev. C **79**, 034310 (2009).

[50] X. Roca-Maza, G. Colò, and H. Sagawa, New Skyrme interaction with improved spin-isospin properties, Phys. Rev. C **86**, 031306(R) (2012).

[51] J. Erler, P. Klüpfel, and P.-G. Reinhard, Exploration of a modified density dependence in the Skyrme functional, Phys. Rev. C **82**, 044307 (2010).

[52] W. Satuła, R. A. Wyss, and M. Rafalski, Global properties of the Skyrme-force-induced nuclear symmetry energy, Phys. Rev. C **74**, 011301(R) (2006).

[53] J. Birkhan, M. Miorelli, S. Bacca, S. Bassauer, C. A. Bertulani, G. Hagen, H. Matsubara, P. von Neumann-Cosel, T. Papenbrock, N. Pietralla, V. Yu. Ponomarev, A. Richter,

A. Schwenk, and A. Tamii, Electric Dipole Polarizability of ^{48}Ca and Implications for the Neutron Skin, Phys. Rev. Lett. **118**, 252501 (2017).
[54] A. Tamii (private communication).
[55] K. Schelhaas, J. Henneberg, M. Sanzone-Arenhvel, N. Wieloch-Laufenberg, U. Zurmhl, B. Ziegler, M. Schumacher, and F. Wolf, Nuclear photon scattering by ^{208}Pb, Nucl. Phys. **A489**, 189 (1988).
[56] F. Tondeur, M. Brack, M. Farine, and J. Pearson, Static nuclear properties and the parametrisation of Skyrme forces, Nucl. Phys. **A420**, 297 (1984).
[57] P.-G. Reinhard, Skyrme forces and giant resonances in exotic nuclei, Nucl. Phys. **A649**, 305 (1999).
[58] S. Yoshida and H. Sagawa, Neutron skin thickness and equation of state in asymmetric nuclear matter, Phys. Rev. C **69**, 024318 (2004).
[59] L.-W. Chen, C. M. Ko, and B.-A. Li, Nuclear matter symmetry energy and the neutron skin thickness of heavy nuclei, Phys. Rev. C **72**, 064309 (2005).
[60] M. Centelles, X. Roca-Maza, X. Viñas, and M. Warda, Nuclear Symmetry Energy Probed by Neutron Skin Thickness of Nuclei, Phys. Rev. Lett. **102**, 122502 (2009).
[61] B. A. Brown, Neutron Radii in Nuclei and the Neutron Equation of State, Phys. Rev. Lett. **85**, 5296 (2000).
[62] S. Typel and B. A. Brown, Neutron radii and the neutron equation of state in relativistic models, Phys. Rev. C **64**, 027302 (2001).
[63] R. Furnstahl, Neutron radii in mean-field models, Nucl. Phys. **A706**, 85 (2002).
[64] M. Kortelainen, J. Erler, W. Nazarewicz, N. Birge, Y. Gao, and E. Olsen, Neutron-skin uncertainties of Skyrme energy density functionals, Phys. Rev. C **88**, 031305(R) (2013).
[65] P.-G. Reinhard and W. Nazarewicz, Nuclear charge and neutron radii and nuclear matter: Trend analysis in Skyrme density-functional-theory approach, Phys. Rev. C **93**, 051303(R) (2016).
[66] B.-A. Li, B.-J. Cai, W.-J. Xie, and N.-B. Zhang, Progress in constraining nuclear symmetry energy using neutron star observables since GW170817, Universe **7**, 182 (2021).
[67] B. Biswas, Impact of PREX-II, the revised mass measurement of PSRJ0740 + 6620, and possible NICER observation on the dense matter equation of state, Astrophys. J. **921**, 63 (2021).
[68] C. Drischler, R. J. Furnstahl, J. A. Melendez, and D. R. Phillips, How Well Do We Know the Neutron-Matter Equation of State at the Densities Inside Neutron Stars? A Bayesian Approach with Correlated Uncertainties, Phys. Rev. Lett. **125**, 202702 (2020).
[69] R. Essick, I. Tews, P. Landry, and A. Schwenk, Astrophysical Constraints on the Symmetry Energy and the Neutron Skin of ^{208}Pb with Minimal Modeling Assumptions, Phys. Rev. Lett. **127**, 192701 (2021).